Journal of Physics:
Conference Series

PAPER • **OPEN ACCESS**

Capacitance-Voltage Characterization of GaAsBi/GaAs Multiple Quantum Wells Grown by Molecular Beam Epitaxy

To cite this article: Faezah Harun *et al* 2025 *J. Phys.: Conf. Ser.* **3020** 012008

Journal of Physics: Conference Series **3020** (2025) 012008 doi:10.1088/1742-6596/3020/1/012008

Capacitance-Voltage Characterization of GaAsBi/GaAs Multiple Quantum Wells Grown by Molecular Beam Epitaxy

Faezah Harun[1*], Robert D. Richards[2] and John PR David[2]

[1] Electronics Technology Section, British Malaysian Institute, Universiti Kuala Lumpur, Gombak, Malaysia
[2] Department of Electronic and Electrical Engineering, University of Sheffield, Sheffield, United Kingdom

[*]E-mail: faezah@unikl.edu.my

Abstract. Incorporating Bismuth into Gallium Arsenide (GaAs) presents significant potential as a replacement for GaAs or InGaAs in the middle layer of multi-junction solar cells. This is due to its lower lattice strain, which allows for better manipulation and maximization of the total current collected from photovoltaic cells, ultimately enhancing the total power output. This study presents a systematic study of various p-i-n diode structures of GaAsBi/GaAs multiple quantum well (MQW), grown by using molecular-beam epitaxy (MBE). Capacitive-voltage (C-V) characterizations were conducted on these structures by using a multi-frequency LCR meter to analyze the depletion region and doping profile after growth. Data collected from the C-V profiling revealed that bulk capacitance dominates over other parasitic effects. Additionally, the intrinsic i-region width and doping density were determined by using Poisson equation fitting curve. The diodes exhibited doping densities ranging from 1.5×10^{16} cm^{-3} to 5.5×10^{16} cm^{-3} and their i-region width are consistent with the nominal values declared during growth. In conclusion, this material system diodes with different well width were grown and fabricated, exhibiting conventional III-V semiconductor behavior, making them a competitive alternative for related electronic applications.

1. Introduction

1.1 Semiconductor material system selection for solar cells

In the photovoltaic (PV) industry, silicon (Si) panels are widely used due to their affordability and long lifespan. Although Si still dominates as the primary material for PV cells, multi-junction PV cells are emerging as strong competitors, offering higher efficiency and energy capacity in both development and commercial application. To date, Fraunhofer Institute for Solar Energy Systems (ISE) has reported cell efficiency of 47.6% superseding National Renewable Energy Laboratory (NREL) with 47.1% efficiency [1][2]. One common cell structure in both multi-junction PV reported above is indium gallium arsenide (InGaAs). InGaAs sub-cell is usually placed in middle junction solar cell catering near-infrared wavelength range. However, InGaAs may impose lattice mismatching during the growth process due to atoms dislocation between the material and the substrate layer. This mismatching leads to compressive strain that can cause

reduction in overall efficiency [3]. As there is no readily available lattice-matched material for the middle junction in PV structure, an alternative approach involves engineering a III-V material system that introduces lower strain levels within the desired wavelength ranges, thereby enabling higher PV efficiency.

Bismuth (Bi), a group fifteen element from the periodic table, commonly referred to as a group V semiconductor material, is drawing significant attention in the electronics industry, particularly for its use in forming III-V semiconductor alloys due to its material properties. A small addition of Bi to a material system can lower the bandgap energy. Compared to other elements in the same group, such as indium and antimony, Bi exhibits a higher rate of bandgap reduction, approximately 84meV per percent concentration [4]. Unlike nitrogen, which affects the conduction band, Bi modifies the valence band by raising its maximum while preserving electron mobility in the conduction band [5]. This bandgap reduction allows the system to operate at longer wavelengths, making it ideal for applications in spintronics, telecommunications and PV [6-8].

Several studies have successfully integrated Bi into GaAs as a potential alternative to InGaAs for middle junction solar cells. Achieving higher Bi incorporation is possible by using a low growth temperature, typically below 400°C, due to its semi-metallic properties [9,10]. However, the grown sample often exhibits noticeable surface roughness, which can trigger defect-assisted recombination, reducing the lifetime of minority carrier. As a result, dark current density increases, which is detrimental to solar cell performance. Higher dark current leads to efficiency losses and negatively affects the electrical characteristics of the device. Therefore, careful optimization of this parameter is crucial for improving efficiency while maintaining material quality.

1.2 Application of multiple quantum well in solar cells structure

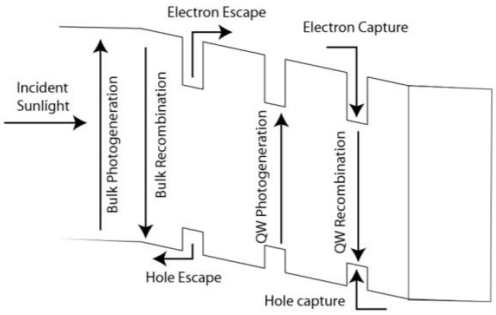

Figure 1. *band diagram for carrier behaviours in MQWs solar cell structures. Images taken from [11].*

Figure 1 shows the carrier behaviour in a MQW p-i-n solar cell. Multiple processes occur simultaneously which are photogeneration and recombination in the quantum well and barrier regions, as well as carrier capture and escape. The carrier capture and escape processes can occur faster than recombination in most quantum well solar cells, at room temperature. For this structure, it is generally assumed that all carriers generated within the quantum well successfully escape and contribute to the photocurrent [11].

To modify the effective bandgap for energy absorption, well structure can be introduced in the growth layer. In addition to that, the carrier energies can be maintained during current extraction in photovoltaic (PV) panels. This approach has demonstrated that integrating quantum

wells into solar cells enables the decoupling of short-circuit current (I_{SC}) and open-circuit voltage ((V_{OC}) [12]. Early investigations on other material such as AlGaAs/GaAs solar cells with MQW structure revealed that the escape of photo-generated carriers from the wells contributed to an increase in output current, thereby improving efficiency compared to reference cells without quantum wells [13]. Furthermore, material such as GaAsP/InGaAs strained MQW p-i-n structures has demonstrated that the collected photocurrent is significantly higher compared to bulk counterparts, leading to improved overall efficiency.

This paper presents the capacitance-voltage (C-V) characterisation of strained-GaAsBi MQW devices as a part of electrical testing for p-i-n structure. Throughout the study, the material system is referred to as (*well/barrier)* devices i.e GaAsBi/GaAs. C-V measurements were conducted to study the device properties, such as depletion region width, built-in potential and doping concentration. A p-i-n structure was chosen due to its simplicity, making it an effective model for predicting semiconductor behavior. The intrinsic (i) layer is particularly important in determining the device performance, and C-V measurements helps in understanding its characteristics. While the intrinsic(i) area is typically undoped with no mobile charge, the carrier distribution in the adjacent doped of p- and n- layers is critical to the overall performance of the device.

2. Methodology

2.1 Device structure

Seven GaAsBi/GaAs MQW p-i-n structure were grown on GaAs substrates using molecular beam epitaxy (MBE). The thickness of the GaAs barriers is adjusted based on the number of wells (8nm thick for each wells), whereas the total i-region thickness is consistently maintained at 620 nm. These devices are labeled as QWXX, where “XX” explains the number of quantum wells in. For instance, QW20 corresponds to the device with twenty wells. The schematic representation of the device structure is illustrated in Figure 2, where “n” signifies the well number and Table 1 shows the nominal barrier thickness for each device with respect to its total well thickness. The growth specifications, fabrication procedures, and other charaterizations of these QWXX devices have been thoroughly detailed in prior research [14-17].

2.2 Experimental method and calculation

C-V measurements were carried out on all devices by applying a reverse DC bias using an LCR meter. Reverse biasing ensures the devices are fully depleted across the i-region, sweeping out any remaining mobile carriers from the depletion region. The capacitance of each device was modelled and calculated using equation (1),

$$C = \frac{I_{AC}}{2\pi f V_{AC}} \quad (1)$$

I_{AC} is the LCR AC test signal, V_{AC} is the AC voltage and f is the test signal frequency. The optimized condition for equivalent circuit model, frequency and AC signal were applied in this measurement setup to achieve accurate readings of capacitance. In this study, the collected data exhibited phase angles between 85° to 90°, suggesting a nearly ideal capacitive behaviour. The recorded data were subsequently plotted and tabulated for the analysis of the devices' electrical properties.

3. Results and Discussion

3.1 C-V measurements

Figure 3(a) presents the C-V and Figure 3(b) is the capacitance with respect to unit area versus voltage (CA-V) measurements for cells with 200 μm and 100 μm radii from the QW20 and QW63 devices. These two devices were selected for comparison due to their distinct characteristics, with QW20 representing a strained device and QW63 being strain-relaxed within the QWXX series. A strained device, such as the QW20, refers to a condition in which the lattice structure of the material accommodates atomic size differences between elements, such as arsenic and bismuth, while maintaining structural integrity. In this case, the strain occurs due to the mismatch in atomic radii between arsenic and bismuth, requiring the crystal lattice to adjust and compensate for the difference without breaking the bonds. On the other hand, a strained-relaxed device like the QW63 exhibits bond breakage within the semiconductor structure due to the excessive strain accumulated from a high number of quantum well layers. As the number of

layers increases, the mismatch in lattice constants between different materials leads to a build-up of strain energy. If this strain exceeds the critical limit that the crystal lattice can sustain, the material undergoes relaxation, causing dislocations and defects to form. These defects act as non-radiative recombination centers, degrading the device performance by reducing carrier mobility and lifetime. As the result, the dark current appear higher [14].

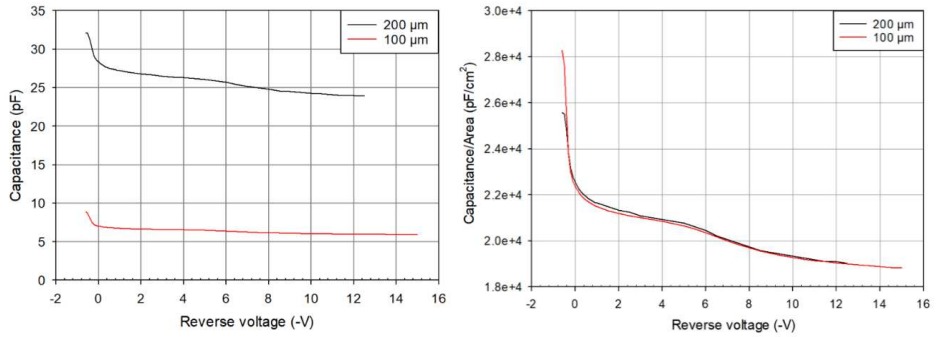

(a)

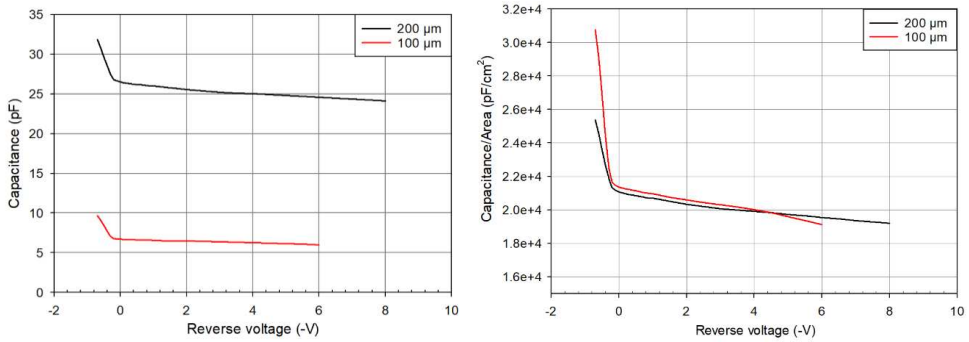

(b)

Figure 3. The *C-V and CA-V for (a) QW20 device and (b) QW63 device. These two devices behave as strained device and strain-relaxed devic, respectively.*

It is assumed that data from devices not shown above follow a similar trend unless stated otherwise. The value of CA-V for both QW20 and QW63 scale show proportionality to the cell area, regardless of variations in strain, this indicates that bulk capacitance primarily governs the measurements. The impact of parasitic effects, including stray capacitance and shunt resistance, is minimal, ensuring that these factors do not significantly influence the overall capacitance of the devices.

3.2 Doping density profile

The background doping density and thickness in the i-region can be tabulated from the raw data. This is achieved by applying a modified one-dimensional Poisson equation to calculate the doping density, N_d as shown in equation (2). From the equation, ε_0 is the dielectric constan valuet, ε_r is the relative constant of the GaAsBi, e is the electron charge and A is the device area,.The

$\mathcal{E}_r$ used is 12.9, similar with GaAs value. A detailed step-by-step derivation of this equation ca be found in [15]:

$$N_d = \frac{2}{\varepsilon_o \varepsilon_r e A^2} \left(\frac{dV}{d\left(1/C^2\right)} \right) \tag{2}$$

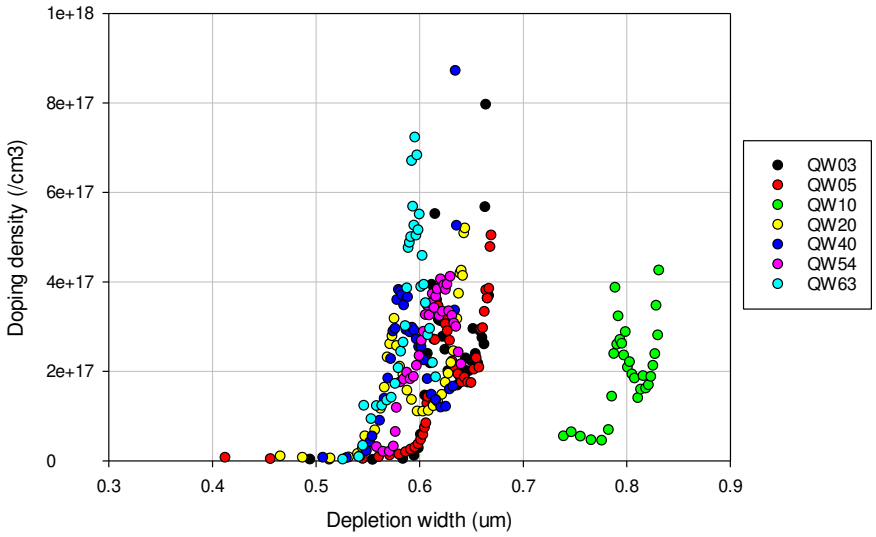

Figure 4. *Doping profile of QWXX devices calculated from C-V curves and modified equation.*

The plotting of doping density (N_d) against the depletion width, x reveals the point along the depletion width where the i-region is fully depleted of mobile carriers in the i-region. The full doping profiles for the QWXX devices are presented in Figure 4.

From the figure, all devices show a sharp increase in doping density, with the measured i-region thickness ranging from 0.55-0.64 μm, indicating that full depletion occurs at zero bias. These values are consistent with the target thickness of 0.62 μm (620nm) set during the growth process for the i-region. The slight variations between these devices are likely due to dopant diffusion during growth. An exception is observed in the QW10 device, where a wider depletion width of approximately 0.75 μm is recorded. The shift of 20nm compared to other QWXX devices is attributed to variations in growth conditions. The first barrier is thicker than others due to a different growth condition [14]. In a p-i-n structure, the depletion width from the i-layer thickness does not affect the doping density of p or n regions, hence the doping profile for QW10 is similar with other QWs in this study. However, note that the difference in width will significantly affects electrical properties such as breakdown voltage and carrier transport.

The value of doping density for the QWXX devices range from approximately 1.5×10^{16} cm^{-3} to 5.5×10^{16} cm^{-3}. These values are consistent with previous studies conducted, where doping densities of 1.2×10^{16} cm^{-3} and 5×10^{16} cm^{-3} were reported for Bi compositions of 2.1-3.4% and 6%, respectively [18,19]. However, the doping level in this study are notably higher compared to other MQW devices, such as InGaAs MQWs, which have been reported to exhibit doping concentrations

below 3×10^{15} cm^{-3} [20]. A high background doping will introduce more free carriers and causing higher recombination rates within the intrinsic region. As the result, the carrier lifetime may decrease and become inefficient in application like solar cells and photodetectors. Besides that, high background doping leads to more generation-recombination centres, increasing reverse leakage currents in the structure and degrading its performance in devices like photodiodes and power rectifiers. Factors such as impurities present in the growth cells and outgassing from the growth chamber may also contribute to the higher doping level observed. Although the specific nature of background doping in this study is not yet fully determined, previous reports have documented undoped GaAsBi exhibiting both p-type [21,22] and n-type [18] background doping. Further investigation would be necessary to determine the specific doping type in these samples.

4. Conclusions

In conclusion, a series of GaAsBi/GaAs MQW p-i-n diodes underwent a C-V measurements as a part of electrical characterisations. The results show that all devices has > 90% depletion rate at zero bias. This behaviour is particularly significant for solar cells applications, as it ensures efficient charge separation through the built-in voltage within the depletion region, enabling charge collection without requiring an external voltage source. Furthermore, operation at zero bias demonstrates that the material can operate as a passive energy-harvesting system without any external energy input. The i-region thicknesses calculated are similar to the nominal value of 0.62 μm, except QW10, which shows a larger thickness of 0.74 μm. All devices exhibit high background doping level in the i-region ($\sim 10^{16}$ cm^{-3}), similar to those reported in other C-V studies on Bi-based materials, though higher that those observed in systems such as InGaAs MQWs. Although the specific type of background doping remains unresolved, data presented in this paper are consistent with previous research on similar materials, and successfully characterizing the quantum well structures. Understanding the electrical characteristics of these p-i-n structures is important for identifying gaps and areas for improvement in Bi-based material systems, such as in terms of growth conditions, material quality and absorption performance. These insights contribute to optimizing the efficiency of multi-junction solar cells where Bi-based layers can play a significant role.

Acknowledgement

Authors would like to thank Universiti Kuala Lumpur (UniKL) for the funding support and gratefully acknowledge Sheffield Bismide Semiconductors Research Group for the valuable discussion and research facilities provided.

References

1. Fraunhofer ISE, "Fraunhofer ISE Develops the World's Most Efficient Solar Cell with 47.6 Percent Efficiency," press release, May 30, 2022. [Online]. Available: https://www.ise.fraunhofer.de/en/press-media/press-releases/2022/fraunhofer-ise-develops-the-worlds-most-efficient-solar-cell-with-47-comma-6-percent-efficiency.html
2. National Renewable Energy Laboratory, "NREL Six-Junction Solar Cell Sets Two World Records for Efficiency," press release, Dec. 2020. [Online]. Available: https://www.nrel.gov/news/press/2020/nrel-six-junction-solar-cell-sets-two-world-records-for-efficiency.html
3. Gu, L., Meng, J. The Influence of Growth Parameters of Strain InGaAs Quantum Wells on Luminescent Properties. *J. Electron. Mater.* **51**, 1421–1427 (2022). https://doi.org/10.1007/s11664-021-09394-6
4. S. Tixier *et al.*, "Molecular Beam Epitaxy Growth of GaAs1-xBix,", *Applied Physics Letters,* Article vol. 82, no. 14, pp. 2245-2247, Apr 2003, doi: 10.1063/1.1565499

5. K. Alberi, O. D. Dubon, W. Walukiewicz, K. M. Yu, K. Bertulis, and A. Krotkus, "Valence Band Anticrossing in $GaBi_xAs_{1-x}$,", *Applied Physics Letters,* Article vol. 91, no. 5, p. 3, Jul 2007, Art no. 051909, doi: 10.1063/1.2768312.
6. Sweeney, S. J. *et al*., The potential role of bismide alloys in future photonic devices. In 13th *International Conference on Transparent Optical Networks*, (IEEE) (2011).
7. Marko, I. P. & Sweeney, S. J., Progress toward III–V bismide alloys for near-and midinfrared laser diodes. *IEEE J. Sel. Top. Quantum Electron.* **23**(6), 1–12 (2017).
8. Thomas, T. *et al.* Requirements for a GaAsBi 1 eV sub-cell in a GaAs-based multi-junction solar cell. *Semicond. Sci. Technol.* **30**(9), 094010 (2015)
9. Young, E. C. *et al.* Bismuth incorporation in GaAs1–xBix grown by molecular beam epitaxy with in-situ light scattering. *Phys. Status Solidi C* **4**(5), 1707–1710 (2007).
10. F. Harun *et al*., "Effect of bismuth flux on the optical and morphological properties of GaAsBi grown by Molecular Beam Epitaxy," *2022 IEEE 8th International Conference on Smart Instrumentation, Measurement and Applications (ICSIMA)*, pp. 127-131, doi: 10.1109/ICSIMA55652.2022.9929153.
11. N.J.Ekins-Daukes *et al.*, "Physics of Quantum Well Solar Cells," in *SPIE - The International Society for Optical Engineering*, 2009, vol. 7211, doi: 10.1117/12.816946.
12. K. W. J. Barnham and G. Duggan, "A New Approach to High-Efficiency Multi-Band-Gap Solar-Cells," *Journal of Applied Physics,* Article vol. 67, no. 7, pp. 3490-3493, Apr 1990, doi: 10.1063/1.345339.
13. K. Barnham *et al.*, "Quantum Well Solar Cells,", *Applied Surface Science,* Article; Proceedings Paper vol. 113, pp. 722-733, Apr 1997, doi: 10.1016/s0169-4332(96)00876-8.
14. R. D. Richards, "Molecular beam epitaxy growth and characterisation of GaAsBi for photovoltaic applications," ed, September 2014.
15. F.Harun, "Characterisation of GaAsBi/GaAs Multiple Quantum Wells for Photovoltaic Applications", ed, February 2020
16. F.Harun *et al*., "Opto-Electronic Characterisation of GaAsBi/GaAs Multiple Quantum Wells for Photovoltaic Applications." Solid State Phenomena, vol. 343, Trans Tech Publications, Ltd., 30 May 2023, pp. 99–104. doi:10.4028/p-j0b6ku.
17. F. Harun, R. D. Richards and J. P. R. David, "Effect of biasing under illumination on GaAsBi/GaAs multiple quantum wells for solar cell performance," *2023 IEEE Regional Symposium on Micro and Nanoelectronics (RSM)*, Langkawi, Malaysia, 2023, pp. 40-43, doi: 10.1109/RSM59033.2023.10326943.
18. Z. Z. Zhou, D. F. Mendes, R. D. Richards, F. Bastiman, and J. P. R. David, "Absorption Properties of GaAsBi based p-i-n Heterojunction Diodes," *Semiconductor Science and Technology,* Article vol. 30, no. 9, p. 6, Sep 2015, Art no. 094004, doi: 10.1088/0268-1242/30/9/094004.
19. C. J. Hunter *et al.*, "Absorption Characteristics of $GaAs_{1-x}Bi_x$/GaAs Diodes in the Near-Infrared," *Ieee Photonics Technology Letters,* vol. 24, no. 23, pp. 2191-2194, Dec 1 2012, doi: 10.1109/lpt.2012.2225420.
20. J. P. R. David, Y. H. Chen, R. Grey, G. Hill, P. N. Robson, and P. Kightley, "Effect of Misfit Dislocations on Leakage Currents in Strained Multiquantum-Well Structures," *Applied Physics Letters,* Article vol. 67, no. 7, pp. 906-908, Aug 1995, doi: 10.1063/1.114690.
21. S. Nargelas, K. Jarasiunas, K. Bertulis, and V. Pacebutas, "Hole Diffusivity in GaAsBi Alloys Measured by a Picosecond Transient Grating Technique," *Applied Physics Letters,* Article vol. 98, no. 8, p. 3, Feb 2011, Art no. 082115, doi: 10.1063/1.3557047.
22. G. Pettinari, A. Patane, A. Polimeni, M. Capizzi, X. F. Lu, and T. Tiedje, "Bi-induced p-type Conductivity in Nominally Undoped Ga(AsBi)," *Applied Physics Letters,* Article vol. 100, no. 9, p. 4, Feb 2012, Art no. 092109, doi: 10.1063/1.3690901.